Biotechnology Progress
DOI 10.1002/btpr.2627

Accepted Article

Evaluation of cellular adhesion and organization in different microporous polymeric scaffolds

Amish Asthana[#], Charles McRae White[#], Megan Douglass and William S. Kisaalita*

Cellular Bioengineering Laboratory

College of Engineering

Driftmier Engineering Center

University of Georgia, Athens, GA 30602

*Corresponding Author: williamk@engr.uga.edu;

(706) 542-0835 (phone); (706) 542-0886

Key Words: Cell-based assay, HTS, Hepatic, Scaffold, 3D culture

[#] Authors contributed equally

This article has been accepted for publication and undergone full peer review but has not been through the copyediting, typesetting, pagination and proofreading process which may lead to differences between this version and the Version of Record. Please cite this article as doi: 10.1002/btpr.2627
© 2018 American Institute of Chemical Engineers Biotechnol Prog
Received: Oct 05, 2017; Revised: Jan 18, 2018; Accepted: Feb 15, 2018

This article is protected by copyright. All rights reserved.

Accepted Article

Abstract

The lack of prediction accuracy during drug development and screening risks complications during human trials, such as drug-induced liver injury (DILI), and has led to a demand for robust, human cell-based, in vitro assays for drug discovery. Microporous polymer-based scaffolds offer an alternative to the gold standard flat tissue culture plastic (2D TCPS) and other 3D cell culture platforms as the porous material entraps cells, making it advantageous for automated liquid handlers and high-throughput screening (HTS). In this study, we optimized the surface treatment, pore size, and choice of scaffold material with respect to cellular adhesion, tissue organization, and expression of complex physiologically relevant (CPR) outcomes such as the presence of bile canaliculi-like structures. Poly-L Lysine (PLL) and fibronectin (FN) coatings have been shown to encourage cell attachment to the underlying substrate. Treatment of the scaffold surface with NaOH followed with a coating of FN improved cell attachment and penetration into pores. Of the two pore sizes we investigated (A: 104 ± 4 μm; B: 175 ± 6 μm), the larger pore size better promoted cell penetration while limiting tissue growth from reaching the hypoxia threshold. Finally, polystyrene (PS) proved to be conducive to cell growth, penetration into the scaffold, and yielded CPR outcomes while being a cost-effective choice for HTS applications. These observations provide a foundation for optimizing microporous polymer-based scaffolds suitable for drug discovery.

This article is protected by copyright. All rights reserved.

Accepted Article

1. Introduction

Drug-induced liver injury (DILI) has been one of the major causes of attrition during the drug development and screening process [(1)]. The lack of prediction accuracy with animal models has put an urgent demand for the development of robust, human cell-based, in vitro assays for drug screening. However, cells cultured on flat tissue culture plastic (2D TCPS) do not develop in vivo-like tissue architecture, resulting in loss of differentiation and tissue-specific functions, limiting their use as alternatives to animal testing. Even though human primary hepatocytes are the current gold standard for drug metabolism and toxicity studies [(2)], their short life span, inter-donor differences, cost and limited availability has been an impediment in their use for in vitro screening assays [(3)]. Hepatocellular carcinoma (HepG2) cells, with their unlimited lifespan, present an attractive alternative to primary hepatocytes [(4)]. However, when cultured in 2D, HepG2 cells express low levels of drug metabolizing cytochrome P450 (CYP450) enzymes [(5)] and the receptors that control their expression [(6),(7)], which might lead to poor prediction of toxicity in humans.

3D cell culture platforms offer an alternative and overcome many limitations associated with monolayers by mimicking in vivo-like microenvironmental conditions. Many 3D hepatocyte models have shown the expression of more physiologically relevant structural and functional characteristics, like development of bile canaliculi, albumin production and urea synthesis that are similar to the native liver tissue [(8)] [(9)] [(10)]. As such, human cell based 3D in vitro assays bridge the gap between conventional 2D and animal models, for drug screening applications. Most of the currently used 3D platforms can be classified into three broad categories: hydrogel based,

This article is protected by copyright. All rights reserved.

Accepted Article

scaffold based and spheroid, and their pros and cons have been discussed in detail by Asthana and Kisaalita [11]. However, their lack of adaptability to currently used automated liquid handling and fluorescence signal detection equipment, along with the high costs associated with these assays limits their usability for high-throughput screening (HTS). For example, some of the currently marketed 3D 96-well plates are hydrogel types. It has been observed in our laboratory [12] and by others [13] that up to 24-fold and 5-fold increases in dye concentration and loading times, respectively, may be required to successfully stain cells in hydrogels. In hydrogels of certain compositions, water can bind with polymer chains, creating a rigid area around the mesh that is not accessible to solute or solvent diffusion [14] [15] [16]. Moreover, hydrogels lack a defined geometry and fail to impose any physical constraints on the size of the growing microtissues. These tissues range from being clusters of a few cells to larger tissues that are above the critical size for oxygen diffusion, which might generate an adulterated outcome in response to drug exposure [17]. Spheroid-based HTS platforms have recently gained popularity, with 96 and 384 well spheroid plates coming to the market. However, as with hydrogels, it is difficult to regulate the size of spheroids due to lack of physical constraints, which is especially significant when using cells that are highly proliferative, like tumor and stem cells. Furthermore, loss of cells during medium change presents an issue with reproducibility.

Microporous polymer-based scaffolds offer an attractive alternative, as the cells are entrapped in the pores, making medium change easier and more amenable to automated liquid handlers. Moreover, scaffolds have a more defined geometry and controllable pore sizes that provide a strict spatial control on microtissue size. A more homogenous tissue size and certainty with the lack of or inclusion of hypoxic conditions would result in a more accurate drug response [17]. In

This article is protected by copyright. All rights reserved.

Accepted Article

this study, we optimize a microporous polymer-based scaffold with respect to cellular adhesion, tissue organization, and expression of complex physiologically relevant (CPR) outcomes by investigating and comparing the effects of three important parameters: surface treatment, pore size, and choice of material. Investigation of these parameters is critical to making informed design choices for the development of a high throughput-compatible, 3D polymer-based scaffold.

2. Materials and Methods

2.1 Scaffold fabrication and characterization

The scaffold was fabricated using the salt leaching method routinely used in our laboratory [18]. Briefly, polystyrene (PS) or poly L-lactic acid (PLLA) was dissolved in chloroform, sieved sodium carbonate decahydrate particles were added, and the polymer solution was mixed thoroughly. The casting mixture was composed of 0.2 g PLLA/PS, 2.5 g sodium carbonate decahydrate and 4 ml chloroform. The size range of the salt particles used was 106 – 125 µm (Scaffold A), 218 – 250 µm (Scaffold B) and <63 µm (Scaffold C). 140 µL of the solution was casted in MatTek® glass bottom Petri dishes (well diameter: 10 mm). After evaporation of chloroform, the dishes were leached with water overnight. The scaffold was sterilized in 70% ethanol (1 hour) and UV (30 mins). It was then either coated with 150 µL of 0.01% poly-l-lysine solution or fibronectin (5 µg in 150 µL PBS). For hydrophilicity treatment, it was treated with 0.2 M NaOH for 40 minutes at 40ºC and after washing thrice with water, was sterilized and coated with fibronectin. The porosity of the scaffolds was measured by a modified liquid displacement method [19], using anhydrous ethanol as the displacement liquid. The pore size

This article is protected by copyright. All rights reserved.

distribution of the scaffolds was determined by analyzing scanning electron microscope (SEM) images using ImageJ software from collective top and bottom view images of the scaffolds. Standard protocol for SEM was followed [20]. Images were captured with a FEI Inspect-F SEM (FEI Company, OR).

2.2 HepG2 cell culture

HepG2 human hepatocellular carcinoma cells (HB-8065) (ATCC, VA) were routinely cultured in 75 cm^2 tissue culture flasks in Minimal Essential Medium (MEM) containing 10% heat inactivated fetal bovine serum (FBS), 2.2 g/L sodium bicarbonate, 2 mM l-glutamine and 1 mM sodium pyruvate in 5% CO_2 at 37 °C. For seeding on scaffolds, cells were counted using Millipore Scepter 2.0 handheld automated cell counter and $7x10^5$ cells (in 140 µl medium) were seeded on Scaffold A and B and 2.8 $x10^5$ on Scaffold C. After allowing 4 hours for attachment, fresh growth medium was added to make the total volume to 1.5 ml in each plate. Half medium change was performed daily.

2.3 Transmission electron microscopy (TEM)

Scaffolds were fixed with 2.5% glutaraldehyde for 30 minutes and treated with 1% OsO_4 for 2 hours at room temperature. After step-wise dehydration with ethanol and propylene oxide (PO), samples were treated with 1:1 mixture of PO and Embed812 resin overnight at room temperature. Finally, the samples were embedded in Embed812 resin following standard procedures. Ultrathin sections of 70 – 90 nm thickness were sliced using a Reichert Ultracut S

John Wiley & Sons

This article is protected by copyright. All rights reserved.

Accepted Article

Accepted Article

Ultramicrotome (Leica, Inc., Deerfield, IL), collected onto 200-mesh copper grids and co-stained with uranyl acetate and lead citrate for 10 min each. Observations were undertaken with a Transmission Electron Microscope (TEM) (JEOL JEM-1011, Japan) at a voltage of 100 kV.

2.4 Hematoxylin and eosin (H&E) staining

Fresh scaffolds were embedded in OCT media and 8 μm thick sections were cut using a Thermo Electron Corporation Cryotome. Subsequent washes were performed to remove excess OCT media and hydrate the sections. The nuclear detail was stained using Gill's II hematoxylin, followed by step-wise ethanol dehydration and eosin staining. After treatment with a solution (1:1) of xylene and acetone, followed by 100% xylene, a permanent mounting medium was used to adhere the glass coverslip to the slide.

2.5 Cell Number Determination

Using the PicoGreen® dsDNA quantitation kit, double stranded DNA (dsDNA) was measured and used to determine cell number. Briefly, scaffold samples with cells were washed with PBS, aspirated, and frozen in -80°C for 24 hours. After thawing, 2 mL of cell lysis buffer was added to each sample and incubated at room temperature for 30 minutes. The scaffolds and buffer were then removed from plates, added to 15mL tubes, vortexed briefly, and incubated for another 30 minutes. The tubes were centrifuged at 500xg for 5 minutes to pellet cells and scaffold debris. 100 μL of each sample was added to a 96-well plate, followed by 100 μL of the aqueous working solution of the Quant-iT™ PicoGreen® reagent. After 5 minutes of incubation

This article is protected by copyright. All rights reserved.

at room temperature, the samples were excited at 485 nm and fluorescence intensity was measured at 520 nm using Synergy™ HTX Microplate Reader. For the viability curve shown in Figure 2e, n = 3 independent biological replicates.

2.6 Atomic Force Microscopy (AFM)

The Young's Modulus was acquired by contact mode, using AFM 5500 (Agilent Technologies; Chandler, AZ) with a triangular tip (Vecco, model MSCT-AUHW, k = 0.1 N/m). The deflection sensitivity was calibrated by measuring the slope of a force distance curve acquired using Mica, and converted from voltage to nanometers. The optical microscope was used to choose a minimum of 5 regions of interest for each sample. Triplicate samples of each scaffold were measured for statistical purposes.

3. Results and Discussion

3.1 Effect of surface treatments on cell behavior

The surface properties of substrate are known to strongly influence the adsorption of proteins, which can subsequently regulate cell behavior such as attachment, spreading, migration and proliferation. Polystyrene, being highly hydrophobic, requires surface modification to improve its cellular biocompatibility. We tried three different treatment methods to test their ability to promote cell adhesion and migration into the scaffold: 1) coating with Poly-L Lysine (PLL), 2) coating with fibronectin (FN), and 3) treatment with NaOH followed by coating with FN

John Wiley & Sons

This article is protected by copyright. All rights reserved.

Accepted Article

Accepted Article

(NaOH/FN). Significant differences in cell morphology and spatial distribution were revealed by SEM. Loosely packed tissues, with many single cells still distinguishable, formed on the top surface and inside the pores for all the three treatments after 3 days in culture (Figure 1a-c).

Poly-L-lysine is a positively-charged amino acid polymer which promotes cell adhesion to substrates by enhancing the electrostatic interaction between the negatively charged ions of the cell membrane and the surface. After 3 days, cells grown on PLL-treated scaffolds showed little migration into the pores and started to form aggregates on the top surface, growing over or around pores, leaving exposed plastic (Figure 1a). Numerous floating cells were also observed in the culture medium for these scaffolds, suggesting a lack of initial cell adhesion to the scaffold. In some areas of cultures grown for 6 – 9 days, cells remained single and appeared unhealthy. By day 9, formation of dense aggregates and the presence of exposed plastic suggest that the cohesive forces among cells outweighed the adhesive forces between cells and the PLL-treated substrate (Figure 1g).

Extracellular matrix (ECM) protein coatings have been shown to promote cell attachment and migration on polymeric materials [20] [21] [22]. In this study, FN was particularly chosen to coat the scaffold surface as it has been shown to be the major component required for compact spheroid formation [23]. Also, adhesion in cell-derived matrices was found to be solely dependent on integrin α5β1 [24], which is the major receptor for FN. Additionally, FN can adsorb to both hydrophilic as well as hydrophobic surfaces [25], making it an attractive option for coating hydrophobic PS. However, adsorption of FN to highly hydrophobic surfaces can result in a loss of activity due to the adoption of an inactive filamentous structure [26] [27]. Scaffolds coated with

This article is protected by copyright. All rights reserved.

FN appeared to promote a more homogenous spatial distribution of single cells on day 3 (Figure 1d). However, the presence of floating cells in culture medium (day 3) and exposed plastic (day 9) similar to PLL-treated scaffolds support previous reports [26] [27] of less cell adhesion due to the denatured form of FN. Floating cells in culture medium can lead to lack of reproducibility in terms of using automated liquid handlers in HTS applications.

It has been shown that NaOH treatment can oxidize PS which results in the availability of hydroxyl groups on its surface [28]. Additionally, FN has been known to have a high propensity to bond with hydroxyl groups [25]. Cultures grown on NaOH/FN-treated scaffolds spread across and into the pores and appeared more organized than cells grown on the scaffolds with the other treatments (Figure 1c, f, i). A homogenous spatial distribution on the top surface of the NaOH/FN-treated scaffold was observed after only 3 days, with a lack of individual cell boundaries indicating the formation of a compact tissue layer (Figure 1c). Pore walls covered with single cells suggested improved initial cell adhesion, although some exposed plastic was still observed. Over time, compact tissue formation progressed on the top surface of the scaffolds and along the inner walls of the pores, completely filling most by day 9 (Figure 1i). Cultures grown on NaOH/FN-treated scaffolds maintained a homogenous spatial distribution throughout all time points, suggesting a combined treatment of NaOH/FN promotes both cohesive and adhesive forces.

3.2 Effect of pore size on cellular organization

John Wiley & Sons

This article is protected by copyright. All rights reserved.

Accepted Article

Accepted Article

To achieve a homogeneous tissue model for drug discovery while preventing hypoxia, the scaffold should have a homogeneous porous structure. It should also have structural integrity while being thin enough to allow adequate diffusion of nutrients and gases in order to avoid areas of cellular necrosis. Finally, cells must perceive a space as 3D to grow effectively. Voids in the scaffold that are too large might result in cells identifying the space as 2D. However, the pore size must be such that it enables entry of cells into the 3D lattice of the material [29]. Therefore, to achieve a homogenous pore size distribution, we slightly modified the fabrication procedure for PS scaffolds developed and routinely used in our laboratory [18]. Briefly, sodium carbonate decahydrate was used as the porogen instead of ammonium bicarbonate. Ammonium carbonate, which has a density of 1.586 g/cm^3 tends to settle down and forms clusters in the bottom layer of the scaffold, resulting in larger and higher number of pores in the lower layers compared to the top layer. Sodium carbonate decahydrate (density - 1.46 g/cm^3) particles tend to remain suspended in the solution, maintaining a homogeneous pore size and pore number distribution throughout the scaffold. Usage of sodium carbonate decahydrate gave rise to a scaffold with a homogenous top and bottom pore size distribution, as shown in Table 1. Student's t-test showed that the difference in pore size between the top and bottom surface for both the scaffolds was not significant ($p>.05$). To determine the effect of pore size on tissue organization and morphology, scaffolds with two distinct pore sizes were fabricated by using sieved particles ranging in size from 106 – 125 μm (Scaffold A) and 218 – 250 μm (Scaffold B). Figure 2a and c show SEM images of blank Scaffold A and B, respectively. The porosity of the 3D scaffolds was determined by liquid displacement method to be 89%. The average pore size of Scaffold A and B was found by the analysis of SEM images to be 104 ± 4 μm (n = 13) and 175 ± 6 μm (n = 10), respectively. The size of the pores was found to be smaller than that of the salt particles used, probably due to

This article is protected by copyright. All rights reserved.

shrinkage of PS during chloroform evaporation. These pore size ranges were chosen with respect to the size of the cells seeded onto the scaffolds. Smaller pores prevented cell invasion, while bigger pores (>200 μm) are more identical to 2D surfaces [30]. To determine the stiffness, Atomic Force Microscopy (AFM) was used to estimate the Young's Modulus values for the two scaffolds, as listed in Table 1. The values were found to be similar for both the scaffolds, and pore size did not significantly affect the stiffness. However, they were significantly lower than the modulus of bulk PS (3 – 3.56 GPa) [31] and closer to that of electrospun PS fibers (3.86 – 16.25 MPa) [32].

Scaffold A and B were NaOH/FN treated as this had proven to be the best method to promote cell adhesion, in the previous section. After 3 days of culture, cells created a homogeneous layer of tissue on top that extended down into the pores (Figure 2 b, d). Cells attached around the circumference of the pore in both the scaffolds; however, in Scaffold B more cells were observed in the bottom of the pores compared to Scaffold A (Figure 2d). This can be attributed to a lack of adequate cell penetration due to the smaller Scaffold A pore diameter and an increased surface area for cell attachment on the top of the scaffold [33] [34]. As the cells settle onto Scaffold A, the smaller pores are quickly closed off by the loose network of cells, leading to fewer cells settling inside the pore. In some pores, cells could be seen extending across voids to make connections with other cells. This closing-off of the pores could lead to transport issues in the later days of culture. In contrast, the pores in Scaffold B were rarely closed off, despite improved cell penetration. By focusing into an open pore on day 3, it was apparent that a larger pore size was more conducive to cell penetration by the presence of cells around the circumference and at the bottom of the pores. In most cases, the pores in Scaffold B were still found to be open by days 6

John Wiley & Sons

This article is protected by copyright. All rights reserved.

Accepted Article

Accepted Article

and 9 despite continual tissue development. Although we cannot conclusively state which pore size is better for overall cell health, we have confidence in our Scaffold B model for a few reasons. A mean homogeneous porous structure of 175 μm limited tissue growth from reaching the hypoxia threshold [17]. The larger pores in Scaffold B better promoted cell migration into the scaffold, and were large enough that most pores remained open over time allowing for nutrient transport.

Cell viability via DNA quantification showed that there was a continuous decrease in viability until the cell number became relatively constant around 96 hours for both the scaffolds (Figure 2e). A high cell density was chosen to seed the scaffolds so that the cells fill the pores and form tissues as soon as possible. This might have led to growth arrest of cells due to contact inhibition, driven by the development of extensive cell to cell contacts and the physical constraint imposed by the pore size on the growth of the microtissues. This behavior is consistent with other studies where cell proliferation rate in 3D has been shown to be lower than 2D, while the expression of cyclin dependent kinase inhibitors (CDI) p21 is higher [35]. Furthermore, when cultured in 3D, HepG2 cells have shown hallmarks of hepatocytes in vivo, with reduced proliferation being one of them [36]. The tissues lose their proliferative capability when they achieve a more differentiated or re-differentiated state with increase in culture time. This decrease in viability or "cell retention" was found to be consistent with other studies where hepatocytes cultured on different 3D platforms, such as porous nano-fibrous PLLA scaffold [37], alginate scaffold [38], electrospun fibers [39], and HepG2 cells grown as spheroids [36] have shown a similar behavior. Paired Student's t-test showed that the cell viability was not significantly different over the time of culture (8 days) between the two scaffolds.

This article is protected by copyright. All rights reserved.

Accepted Article

The interstitial part of the scaffold between the pores is not flat like 2D TCPS; instead, the bulk material has micropores that are smaller in size compared to those produced by salt leaching. It was unclear how the cells that did not migrate into the pores but attached to the non-porous part of the scaffold would behave. To recreate this surface type, we fabricated Scaffold C using a smaller salt particle size (< 63 μm). This yielded a scaffold with pore size of 14 ± 1 μm (Figure 3a), so that the cells could not migrate into the pores, rather attached on top of the surface, therefore being analogous to the cells that did not migrate into the pores in Scaffold A and B. SEM analysis of cells grown on Scaffold C revealed two distinct cell morphologies: flat and round (Figure 3b). Individual cells interacting directly with the scaffold appeared flat, while cells separated from the scaffold by an aggregate appeared round. Concurrent TEM analysis of this scaffold on day 6 of culture revealed the presence of bile canaliculi-like structures between the cells (Figure 3c). The differences in individual cell morphology coupled with the presence of a structural marker for CPR suggested that these cells behaved in a physiologically relevant manner.

3.3 Effect of polymeric material on cellular organization

PLLA and its derivatives have traditionally been the materials of choice for fabricating tissue-engineering scaffolds due to their amenability to surface treatments, higher wettability and higher surface roughness. In addition, PLLA can be made nanofibrous by including a phase separation step during the fabrication process [(40)]. In the past, PLLA has been used in our lab to fabricate various scaffolds for supporting three-dimensional growth of cells. We observed that

This article is protected by copyright. All rights reserved.

Accepted Article

even in the absence of phase separation during fabrication, PLLA showed the presence of two different nanostructures along with areas that were comparatively smooth (Figure 4a inserts). This can also be due to the treatment of the scaffold with NaOH. Alkaline hydrolysis has been shown to not just increase the surface wettability and hydrophilicity [41] but it also changes the structure, leading to an increase in surface roughness [42]. The dimensions of these structures were analogous to collagen fibers that vary in diameter from 50 to 500 nm; therefore, they might be mimicking collagen on a molecular level [43].

After optimizing surface treatment and pore size for the best initial cellular attachment and organization, we decided to study the behavior of HepG2 cells growing on PLLA scaffolds to determine the role of platform material in tissue organization and morphology. A porous PLLA scaffold was prepared using the same process as with PS, treated with NaOH and coated with FN. HepG2 cells were cultured for up to 9 days, fixing samples for SEM on days 3, 6 and 9. By day 3, cells on PS had formed homogenous, compact tissue made evident by the lack of individual cell boundaries (Figure 4e). Tissue formation extended across the top surface and down the pore walls, leaving a central void that made pore identification easy. The diameters of these voids were smaller than the pore diameter of a blank scaffold, suggesting that cells grew around the circumference of the pores. Over time, these void diameters become even smaller (Figure 4f), suggesting that the cells filled the pores in an outside-in manner on PS scaffolds.

Interestingly, cells grown on PLLA scaffolds appeared to fill pores in a different manner. While most pores were not completely filled in PS scaffolds (even by day 9), a loose network of cells had occupied the pores and seemed to completely fill them in an inside-out manner in PLLA

This article is protected by copyright. All rights reserved.

scaffolds by day 3 (Figure 4b). They formed compact tissues by day 6 (Figure 4c), making pore identification difficult by day 9 (image not shown). Although both pore sizes (A and B) were used for comparison of PS and PLLA, the inside out attachment of cells on PLLA was more apparent in Scaffold A. This might be because Scaffold B shows improved cell penetration. By day 6, the pores are completely filled, making it difficult to observe how cells fill and occupy the pores over time. With Scaffold A, however, more cells attach initially to the top surface of the scaffold instead of penetrating to the center, revealing the difference in cell attachment between materials.

We hypothesize that this differential attachment and organization of cells on the two materials is due to the difference in the nanostructure of the scaffolds, which is evident in SEM images at a high magnification (Figure 4a, d inserts). While PS mostly appeared smooth and pores could simply be classified as voids in the material, PLLA had a nanotexture that gave pores a more complex structure. Many studies have shown that cells can sense the presence and react to micro and nanofeatures like islands, pits, ridges and columns by modulating their cytoskeleton, which leads to differences in adhesion, orientation and directional migration [44] [45] [46]. These studies have also shown the presence of multiple broad (lamellipodia) and spike-like (filopodia) protrusions, sensing and interacting with these topologies. These protrusions, driven by the polymerization of actin filaments, are central to cell-substrate interactions, providing the driving force for cell migration in response to chemo-attractants as well as directional cues [47]. In our PLLA scaffolds, the presence of such protrusions interacting with the nanotopologies could not be seen due to the way the cells organize themselves in the pores, making it hard to observe cell-substrate interaction using SEM (Figure 4b). However, as there is a void at the bottom of the

John Wiley & Sons

This article is protected by copyright. All rights reserved.

Accepted Article

pores in PS scaffolds, both lamellipodia and filopodia were observed penetrating microporous structures (1 – 5 μm diameter; Figure 4g). In the absence of surface roughness or nanostructures in PS scaffolds, it seems, the cells have a propensity to initially migrate and attach to the walls of the pores rather than the bottom. Subsequently more cells attach to this initial outer layer of cells and try to fill the pores in a circumferential manner. To confirm the SEM observations on surface topography, AFM was used in Acoustic AC mode (AAC) to obtain high-resolution topographic images of the scaffolds. Figure 4h and i show the 3D topographical images of a 1.2 x 1.2 μm^2 area scan of NaOH-treated PS and PLLA scaffolds, respectively. A difference in surface roughness between the two polymers was observed at the nanolevel, with the root mean square (RMS) roughness being 1.6516 for PS and 4.9384 nm for PLLA. Therefore, we speculate that cells can sense the nanotexture of the PLLA scaffold, which leads to the difference in cell alignment and tissue organization between the two scaffolds.

Since PLLA is biodegradable under culture conditions, which can be even faster when the scaffold is porous and thin, it might not be desirable for long-term culture of cells in vitro. It should also be noted that HepG2 tissues grown on both the scaffolds showed presence of physiologically relevant structural outcomes like bile canaliculi development, which is prerequisite for their application in drug screening and toxicology studies. On the other hand, PS is non-degradable and comparatively cheaper than PLLA which might make it a better choice of material for the development of 3D platforms, as cost of such platforms (compared to 2D TCPS) is a major deterrent for the industry to adopt 3D for drug discovery applications.

3.4 Structural assessment of cells

This article is protected by copyright. All rights reserved.

Accepted Article

Accepted Article

One of the basic structural phenomena that distinguish liver cells in the native tissue from those cultured in 2D formats is polarity. While those in their natural environment possess structural and functional polarity [48] [49], ones that are isolated and cultured on most flat non-porous surfaces do not [50] [51]. Most hepatic functions like biliary excretion, albumin secretion and urea synthesis are thought to be dependent on the polarized phenotype of the cells. In their native conditions, hepatocytes maintain a cuboidal shape and the lateral domain between adjacent cells is divided by a polygonal network of microvilli-lined bile canaliculi. The ultra-structure of HepG2 tissues cultured on the scaffolds was examined by TEM (Figure 5a). The presence of microvilli-lined bile canaliculi-like structures was observed in tissues growing on scaffolds across all conditions. A network of microvilli-lined channels was seen on day 6, distinguished by multiple tight junctions. The presence of a wide range of organelles, typically found in most mammalian cells, was also observed in all scaffolds. Cell viability and organization was evaluated by hematoxylin and eosin (H&E) which stains the cytoplasm pink and nucleus blue (Figure 5b). HepG2 cells cultured on Scaffold B, which was NaOH/FN treated, showed intact cytoskeleton with high viability and no signs of necrosis on day 6 of culture. The cells had formed compact microtissues within the scaffold pores, establishing cell-cell contacts and development of canaliculi-like openings and a network of channels. Furthermore, SEM analysis of the scaffold showed frequent opening of the channels on the surface of the microtissue (Figure 5c). The diameter of the openings was found to be 1 – 2 μm, which is consistent with prior reports of dimensions of bile canaliculi observed in 3D HepG2 (2 – 3 μm) [52] and primary rat hepatocyte (1 – 3 μm) [53] spheroid cultures.

This article is protected by copyright. All rights reserved.

Accepted Article

As the pliability of synthetic polymers is above the physiological range, it is usually assumed that they fail to provide optimum biophysical cues for the cells, in comparison to softer hydrogels that provide a more physiological biophysical microenvironment. Considering that the microporous scaffolds provide a sub-optimal microenvironment, the liver cells grown on them were expected to produce an aberrant or at least a significantly different outcome compared to hydrogel cultures. However, we observed microvilli-lined bile canaliculi-like structures on both the polymers, which is a CPR outcome for cells of hepatic origin. This is in accordance with other studies where hepatic cells grown on PS [29] [54] and PLLA [37] scaffolds have shown the presence of these structures and higher albumin production (functional CPR) [37] compared to 2D cultures. We hypothesize that this lack of pliability effect comes from the "cell-on-cell" hypothesis [55], where cell-cell contacts appear to play a more pivotal role as neighboring cells provide a soft "stroma" for surrounding cells and produce responses similar to cells that are grown in softer gels. It has been well established that cells can sense and attempt to replicate the stiffness of their substrate in 2D [56]. When cells are seeded at a high density, as in the case of the scaffold, the sheer number of cell-cell interactions might supersede the fewer cell-substrate interactions, leading to the formation of a cohesive microtissue such that only the outermost tissue layer is in contact with the substrate while others are exclusively in contact with tissue. We suspect that this overwhelming number of cell-cell interactions might have minimized the effect of the substrate mechanical properties, once a compact tissue was formed. Several flat cells with cell-substrate adhesions were observed, while additional single cells that adhered on top of them only perceived the flat cells underneath. Similar to the results published by Discher *et al* [55], the top cells had a markedly different morphology compared to the flat cells with which they were interacting. The bottom cell layer had a noticeably higher surface area per cell, like

This article is protected by copyright. All rights reserved.

Accepted Article

those grown on rigid 2D surfaces [56], while the top cells had a native, round morphology (Figure 5d).

4. Conclusions

The architectural design and surface treatment of scaffolds can affect the cellular organization after seeding, development of homogeneous tissues over time, mass transport of nutrients, and development of structural markers for CPR. The compatibility with standard assay plates and automation equipment makes this scaffold fabrication approach suitable for high-throughput toxicity screening. After extensive characterization, the results support the following conclusions:

- Treatment of the scaffold with NaOH coupled with the coating of ECM protein Fibronectin promoted better cell attachment and homogenous spatial distribution of cells
- A bigger pore size (Scaffold B; 175 ± 6 μm) was found to be more favorable for cell penetration into PS scaffolds
- PS Scaffold B was conducive to cell growth, penetration into the scaffold, and yielded complex physiologically relevant outcomes (CPR) while being a cost-effective choice for drug discovery and HTS applications.

These observations provide an initial basis for optimizing 3D polymer-based scaffolds suitable for HTS applications.

This article is protected by copyright. All rights reserved.

Accepted Article

Figure Captions

Figure 1. Qualitative investigation of the effects substrate surface properties has on cell adhesion, tissue development, morphology and viability. SEM micrographs of HepG2 tissues grown on PS scaffolds treated with PLL (a, d, g) FN (b, e, h) and NaOH/FN (c, f, i) taken on days 3, 6 and 9 (rows 1, 2, and 3, respectively). Red arrows indicate exposed plastic while yellow arrows identify single cells. NaOH/FN-treated scaffolds show a homogenous tissue layer as a result of improved cell penetration and attachment.

Figure 2. Characterization of NaOH/FN-treated 3D PS scaffold pore size and subsequent microtissue formation. SEM micrographs of Scaffold A (a, b) with average pore size (104 ± 4 μm, n=13) and Scaffold B (c, d) (175 ± 6 μm, n=10). Cells developed homogenous tissue layer on the top surface of the scaffold while penetrating and closing off pores. The viability curve for cells grown on the two scaffolds (n = 3) shows a decrease in viability over time, which becomes stable from day 4 onwards (e).

Figure 3. HepG2 cell morphology in 2D-like PS Scaffold C. Emulation of the non-porous top surface of our scaffold model (a) reveals cells directly interacting with the scaffold adopt a flat morphology. A round morphology is assumed to be the result of cell-cell interactions, regardless of the mechanical properties of the scaffold (b). Structural characterization of the cells growing on Scaffold C showed formation of microvilli-lined bile canaliculi-like structures (c). White solid arrow – tight junction, white arrowhead – microvilli, M – Mitochondria, N - Nucleus

This article is protected by copyright. All rights reserved.

Figure 4. SEM micrographs of PLLA (a-c) and PS (d-f) scaffolds reveal different mechanisms employed by cell populations to fill pores. Scaffold A with pore size (104μm ± 4μm) was used. HepG2 tissues grown on PS scaffolds fill pores with an "outside-in" manner, while tissues on PLLA form a loose network termed "inside-out". Investigation of high magnification SEM micrographs of blank PLLA (a) and PS (d) scaffolds reveal differences in nanotexture inherent to the manufacturing process. Button- and Rod-like textures on PLLA appear randomly throughout the scaffold, while PS maintains a smooth surface with occasional 1 – 5 μm pores. Lamellipodia and filopodia were observed penetrating microporous structures in PS scaffolds (g). Part h and i show the 3D topographical images of a 1.2 x 1.2 μm^2 area scan of NaOH-treated PS and PLLA scaffolds, respectively, obtained using AFM. A difference in surface roughness between the two surfaces can be observed at the nanolevel.

Figure 5. Structural characterization of HepG2 tissues using TEM (a), H&E (b), and SEM (c). These bile canaliculi-like structures are absent in 2D cultures, and serve as markers for CPR. Microvilli-lined canaliculi were observed using TEM on day 6 of culture (a). Multiple cell-cell junctions and canicular networks were observed in scaffolds. White solid arrow – tight junction, white arrowhead – microvilli, M – mitochondria, N - nucleus. H&E staining on day 6 showed high viability and development of channels (b; white arrows). Frequent opening of the channels on the surface of the microtissue (c). (d & e) show SEM images of HepG2 cell-material and cell-cell interactions on a porous PS scaffold. Consistent with current literature, cells adapt to the stiffness of their environment and adopt a flat, spread out morphology (d). However, cells that interact exclusively with other cells adopt a round morphology, suggesting the cell perceives a softer, in vivo-like stiffness (e).

John Wiley & Sons

This article is protected by copyright. All rights reserved.

Accepted Article

Table 1. Characterization of Scaffolds A and B

	Scaffold A	**Scaffold B**
Salt size (μm)	106 – 125	212 – 250
Pore size – Top (μm)	104 ± 14	175 ± 20
Pore size – Bottom (μm)	91 ± 14	165 ± 22
Porosity (%)	89	89
Young's Modulus (MPa)	8.8 ± 2.3	9.3 ± 3.0

This article is protected by copyright. All rights reserved.

1. MacDonald JS, Robertson RT. Toxicity testing in the 21st century: a view from the pharmaceutical industry. Toxicol Sci. 2009;110(1):40-6.
2. LeCluyse EL. Human hepatocyte culture systems for the in vitro evaluation of cytochrome P450 expression and regulation. Eur J Pharm Sci. 2001;13(4):343-68.
3. Madan A, Graham RA, Carroll KM, Mudra DR, Burton LA, Krueger LA, et al. Effects of prototypical microsomal enzyme inducers on cytochrome P450 expression in cultured human hepatocytes. Drug Metab Dispos. 2003;31(4):421-31.
4. Guo L, Dial S, Shi L, Branham W, Liu J, Fang JL, et al. Similarities and differences in the expression of drug-metabolizing enzymes between human hepatic cell lines and primary human hepatocytes. Drug Metab Dispos. 2011;39(3):528-38.
5. Wilkening S, Stahl F, Bader A. Comparison of primary human hepatocytes and hepatoma cell line Hepg2 with regard to their biotransformation properties. Drug Metab Dispos. 2003;31(8):1035-42.
6. Kanno Y, Inouye Y. A consecutive three alanine residue insertion mutant of human CAR: a novel CAR ligand screening system in HepG2 cells. J Toxicol Sci. 2010;35(4):515-25.
7. Naspinski C, Gu X, Zhou GD, Mertens-Talcott SU, Donnelly KC, Tian Y. Pregnane X receptor protects HepG2 cells from BaP-induced DNA damage. Toxicol Sci. 2008;104(1):67-73.
8. Fey SJ, Wrzesinski K. Determination of drug toxicity using 3D spheroids constructed from an immortal human hepatocyte cell line. Toxicol Sci. 2012;127(2):403-11.
9. Godoy P, Hewitt NJ, Albrecht U, Andersen ME, Ansari N, Bhattacharya S, et al. Recent advances in 2D and 3D in vitro systems using primary hepatocytes, alternative hepatocyte sources and non-parenchymal liver cells and their use in investigating mechanisms of hepatotoxicity, cell signaling and ADME. Arch Toxicol. 2013;87(8):1315-530.
10. Tostoes RM, Leite SB, Serra M, Jensen J, Bjorquist P, Carrondo MJ, et al. Human liver cell spheroids in extended perfusion bioreactor culture for repeated-dose drug testing. Hepatology. 2012;55(4):1227-36.
11. Asthana A, Kisaalita WS. Biophysical microenvironment and 3D culture physiological relevance. Drug Discov Today. 2013;18(11-12):533-40.
12. Mao C, Kisaalita WS. Characterization of 3-D collagen hydrogels for functional cell-based biosensing. Biosens Bioelectron. 2004;19(9):1075-88.
13. O'Connor SM, Andreadis JD, Shaffer KM, Ma W, Pancrazio JJ, Stenger DA. Immobilization of neural cells in three-dimensional matrices for biosensor applications. Biosens Bioelectron. 2000;14(10-11):871-81.
14. Koda S, Yamashita K, Iwai S, Nomura H, Iwata M. Ultrasonic investigation of the states of water in hydrogels. Polymer. 1994;35(26):5626-9.
15. Roorda W. Do hydrogels contain different classes of water? Journal of Biomaterials Science, Polymer Edition. 1994;5(5):381-95.
16. Xu H, Vij J, McBrierty V. Wide-band dielectric spectroscopy of hydrated poly (hydroxyethyl methacrylate). Polymer. 1994;35(2):227-34.
17. Asthana A, Kisaalita WS. Microtissue size and hypoxia in HTS with 3D cultures. Drug Discov Today. 2012;17(15-16):810-7.
18. Cheng K, Lai Y, Kisaalita WS. Three-dimensional polymer scaffolds for high throughput cell-based assay systems. Biomaterials. 2008;29(18):2802-12.
19. Zhang R, Ma PX. Poly (a-hydroxyl acids)/hydroxyapatite porous composites for bone-tissue engineering. I. Preparation and morphology. Journal of biomedical materials research. 1999;44(4):446-55.

This article is protected by copyright. All rights reserved.

20. Tamada Y, Ikada Y. Effect of preadsorbed proteins on cell adhesion to polymer surfaces. Journal of colloid and interface science. 1993;155(2):334-9.
21. Dewez J-L, Lhoest J-B, Detrait E, Berger V, Dupont-Gillain CC, Vincent L-M, et al. Adhesion of mammalian cells to polymer surfaces: from physical chemistry of surfaces to selective adhesion on defined patterns. Biomaterials. 1998;19(16):1441-5.
22. Yamamoto A, Mishima S, Maruyama N, Sumita M. Quantitative evaluation of cell attachment to glass, polystyrene, and fibronectin- or collagen-coated polystyrene by measurement of cell adhesive shear force and cell detachment energy. J Biomed Mater Res. 2000;50(2):114-24.
23. Salmenpera P, Kankuri E, Bizik J, Siren V, Virtanen I, Takahashi S, et al. Formation and activation of fibroblast spheroids depend on fibronectin-integrin interaction. Exp Cell Res. 2008;314(19):3444-52.
24. Cukierman E, Pankov R, Stevens DR, Yamada KM. Taking cell-matrix adhesions to the third dimension. Science. 2001;294(5547):1708-12.
25. Keselowsky BG, Collard DM, Garcia AJ. Surface chemistry modulates fibronectin conformation and directs integrin binding and specificity to control cell adhesion. J Biomed Mater Res A. 2003;66(2):247-59.
26. Iuliano DJ, Saavedra SS, Truskey GA. Effect of the conformation and orientation of adsorbed fibronectin on endothelial cell spreading and the strength of adhesion. Journal of biomedical materials research. 1993;27(8):1103-13.
27. Grinnell F, Feld MK. Adsorption characteristics of plasma fibronectin in relationship to biological activity. Journal of biomedical materials research. 1981;15(3):363-81.
28. Hambardzumyan A, Biltresse S, Dufrêne Y, Marchand-Brynaert J. An unprecedented surface oxidation of polystyrene substrates by wet chemistry under basic conditions. Journal of colloid and interface science. 2002;252(2):443-9.
29. Bokhari M, Carnachan RJ, Cameron NR, Przyborski SA. Novel cell culture device enabling three-dimensional cell growth and improved cell function. Biochem Biophys Res Commun. 2007;354(4):1095-100.
30. Freyman T, Yannas I, Gibson L. Cellular materials as porous scaffolds for tissue engineering. Progress in Materials Science. 2001;46(3):273-82.
31. Jee A-Y, Lee M. Comparative analysis on the nanoindentation of polymers using atomic force microscopy. Polymer Testing. 2010;29(1):95-9.
32. Baker SC, Atkin N, Gunning PA, Granville N, Wilson K, Wilson D, et al. Characterisation of electrospun polystyrene scaffolds for three-dimensional in vitro biological studies. Biomaterials. 2006;27(16):3136-46.
33. Lee M, Wu BM, Dunn JC. Effect of scaffold architecture and pore size on smooth muscle cell growth. J Biomed Mater Res A. 2008;87(4):1010-6.
34. Murphy CM, O'Brien FJ. Understanding the effect of mean pore size on cell activity in collagen-glycosaminoglycan scaffolds. Cell Adh Migr. 2010;4(3):377-81.
35. Birgersdotter A, Sandberg R, Ernberg I. Gene expression perturbation in vitro--a growing case for three-dimensional (3D) culture systems. Semin Cancer Biol. 2005;15(5):405-12.
36. Ramaiahgari SC, den Braver MW, Herpers B, Terpstra V, Commandeur JN, van de Water B, et al. A 3D in vitro model of differentiated HepG2 cell spheroids with improved liver-like properties for repeated dose high-throughput toxicity studies. Arch Toxicol. 2014;88(5):1083-95.

This article is protected by copyright. All rights reserved.

37. Bierwolf J, Lutgehetmann M, Feng K, Erbes J, Deichmann S, Toronyi E, et al. Primary rat hepatocyte culture on 3D nanofibrous polymer scaffolds for toxicology and pharmaceutical research. Biotechnol Bioeng. 2011;108(1):141-50.
38. Dvir-Ginzberg M, Gamlieli-Bonshtein I, Agbaria R, Cohen S. Liver tissue engineering within alginate scaffolds: effects of cell-seeding density on hepatocyte viability, morphology, and function. Tissue Eng. 2003;9(4):757-66.
39. Wang T, Feng Z-Q, Leach MK, Wu J, Jiang Q. Nanoporous fibers of type-I collagen coated poly (L-lactic acid) for enhancing primary hepatocyte growth and function. Journal of Materials Chemistry B. 2013;1(3):339-46.
40. Cheng K, Kisaalita WS. Exploring cellular adhesion and differentiation in a micro-/nano-hybrid polymer scaffold. Biotechnol Prog. 2010;26(3):838-46.
41. Wang L, Kisaalita WS. Characterization of micropatterned nanofibrous scaffolds for neural network activity readout for high-throughput screening. J Biomed Mater Res B Appl Biomater. 2010;94(1):238-49.
42. Park GE, Pattison MA, Park K, Webster TJ. Accelerated chondrocyte functions on NaOH-treated PLGA scaffolds. Biomaterials. 2005;26(16):3075-82.
43. Chen VJ, Ma PX. Nano-fibrous poly(L-lactic acid) scaffolds with interconnected spherical macropores. Biomaterials. 2004;25(11):2065-73.
44. Martinez E, Engel E, Planell JA, Samitier J. Effects of artificial micro- and nano-structured surfaces on cell behaviour. Ann Anat. 2009;191(1):126-35.
45. Dalby MJ, Childs S, Riehle MO, Johnstone HJ, Affrossman S, Curtis AS. Fibroblast reaction to island topography: changes in cytoskeleton and morphology with time. Biomaterials. 2003;24(6):927-35.
46. Dalby M, Riehle M, Johnstone H, Affrossman S, Curtis A. Polymer-demixed nanotopography: control of fibroblast spreading and proliferation. Tissue engineering. 2002;8(6):1099-108.
47. Parsons JT, Horwitz AR, Schwartz MA. Cell adhesion: integrating cytoskeletal dynamics and cellular tension. Nat Rev Mol Cell Biol. 2010;11(9):633-43.
48. Hubbard A, Barr V, Scott L. Hepatocyte surface polarity. The Liver: Biology and Pathobiology. 1994:189-213.
49. Maurice M, Rogier E, Cassio D, Feldmann G. Formation of plasma membrane domains in rat hepatocytes and hepatoma cell lines in culture. Journal of Cell Science. 1988;90(1):79-92.
50. Moghe PV, Berthiaume F, Ezzell RM, Toner M, Tompkins RG, Yarmush ML. Culture matrix configuration and composition in the maintenance of hepatocyte polarity and function. Biomaterials. 1996;17(3):373-85.
51. LeCluyse EL, Audus KL, Hochman JH. Formation of extensive canalicular networks by rat hepatocytes cultured in collagen-sandwich configuration. American Journal of Physiology-Cell Physiology. 1994;266(6):C1764-C74.
52. Lee J, Cuddihy MJ, Cater GM, Kotov NA. Engineering liver tissue spheroids with inverted colloidal crystal scaffolds. Biomaterials. 2009;30(27):4687-94.
53. Abu-Absi SF, Friend JR, Hansen LK, Hu WS. Structural polarity and functional bile canaliculi in rat hepatocyte spheroids. Exp Cell Res. 2002;274(1):56-67.
54. Bokhari M, Carnachan RJ, Cameron NR, Przyborski SA. Culture of HepG2 liver cells on three dimensional polystyrene scaffolds enhances cell structure and function during toxicological challenge. Journal of anatomy. 2007;211(4):567-76.

This article is protected by copyright. All rights reserved.

55. Discher DE, Janmey P, Wang YL. Tissue cells feel and respond to the stiffness of their substrate. Science. 2005;310(5751):1139-43.
56. Solon J, Levental I, Sengupta K, Georges PC, Janmey PA. Fibroblast adaptation and stiffness matching to soft elastic substrates. Biophys J. 2007;93(12):4453-61.

Accepted Article

This article is protected by copyright. All rights reserved.

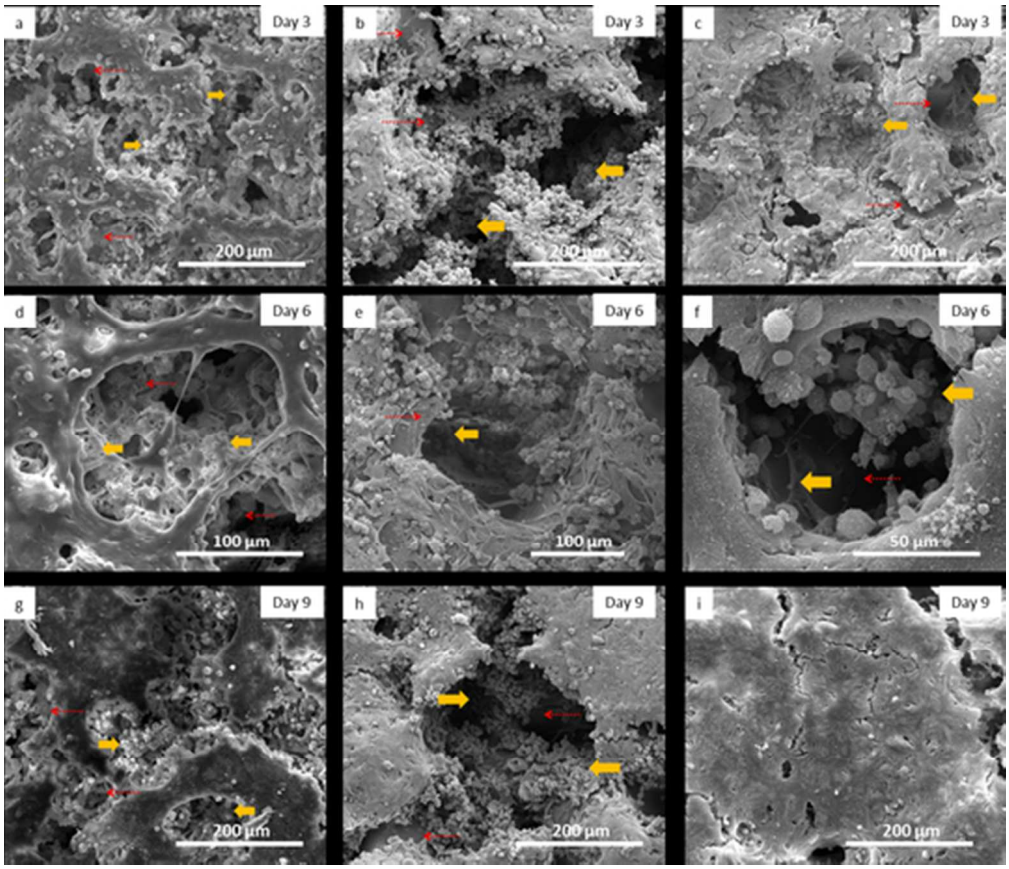

Figure 1. Qualitative investigation of the effects substrate surface properties has on cell adhesion, tissue development, morphology and viability. SEM micrographs of HepG2 tissues grown on PS scaffolds treated with PLL (a, d, g) FN (b, e, h) and NaOH/FN (c, f, i) taken on days 3, 6 and 9 (rows 1, 2, and 3, respectively). Red arrows indicate exposed plastic while yellow arrows identify single cells. NaOH/FN-treated scaffolds show a homogenous tissue layer as a result of improved cell penetration and attachment.

45x39mm (300 x 300 DPI)

Acce

This article is protected by copyright. All rights reserved.

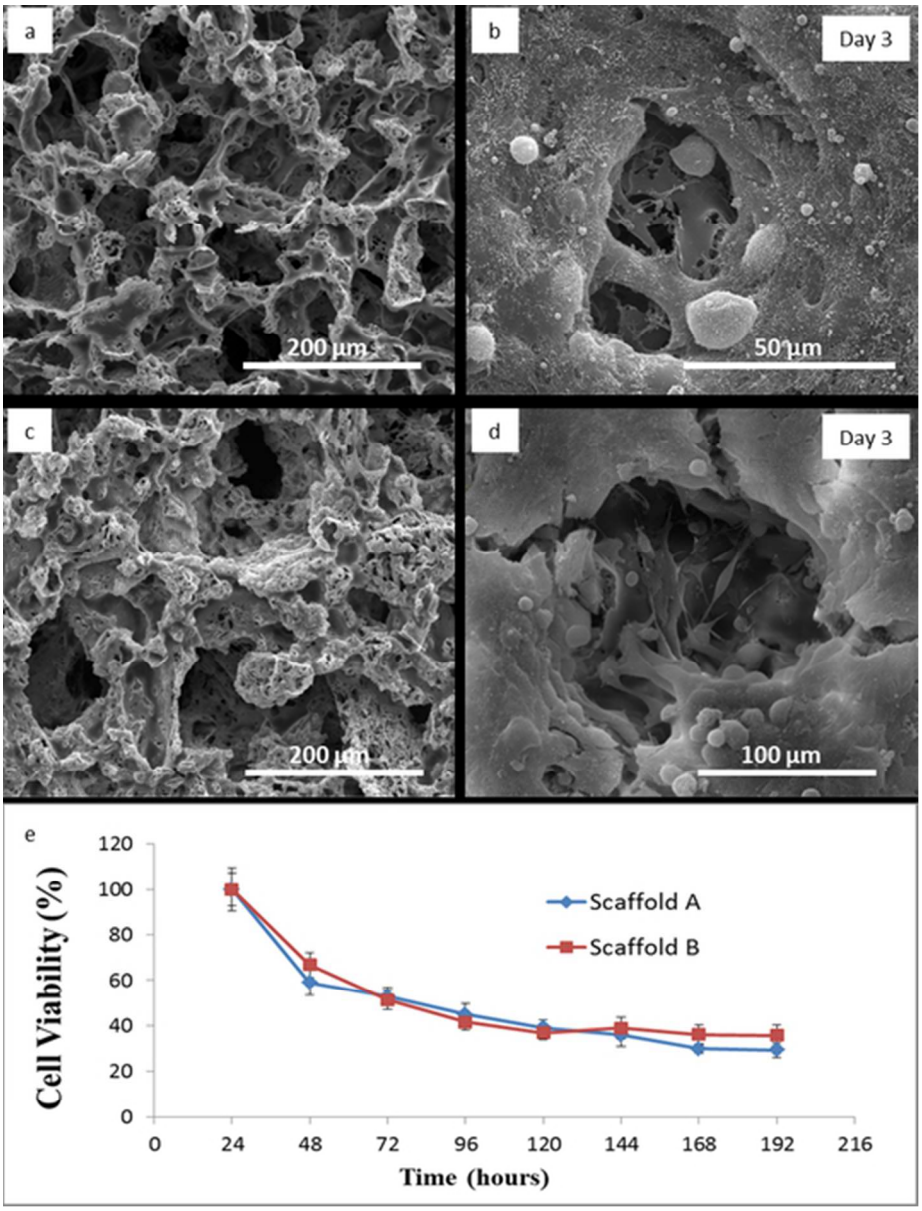

Figure 2. Characterization of NaOH/FN-treated 3D PS scaffold pore size and subsequent microtissue formation. SEM micrographs of Scaffold A (a, b) with average pore size (104 ± 4 µm, n=13) and Scaffold B (c, d) (175 ± 6 µm, n=10). Cells developed homogenous tissue layer on the top surface of the scaffold while penetrating and closing off pores. The viability curve for cells grown on the two scaffolds shows a decrease in viability over time, which becomes stable from day 4 onwards (e).

45x59mm (300 x 300 DPI)

This article is protected by copyright. All rights reserved.

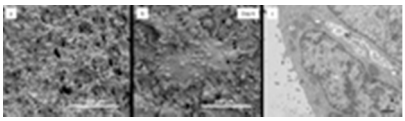

Figure 3. HepG2 cell morphology in 2D-like PS Scaffold C. Emulation of the non-porous top surface of our scaffold model (a) reveals cells directly interacting with the scaffold adopt a flat morphology. A round morphology is assumed to be the result of cell-cell interactions, regardless of the mechanical properties of the scaffold (b). Structural characterization of the cells growing on Scaffold C showed formation of microvilli-lined bile canaliculi-like structures (c). White solid arrow – tight junction, white arrowhead – microvilli, M – Mitochondria, N - Nucleus

16x4mm (300 x 300 DPI)

Accepted Article

This article is protected by copyright. All rights reserved.

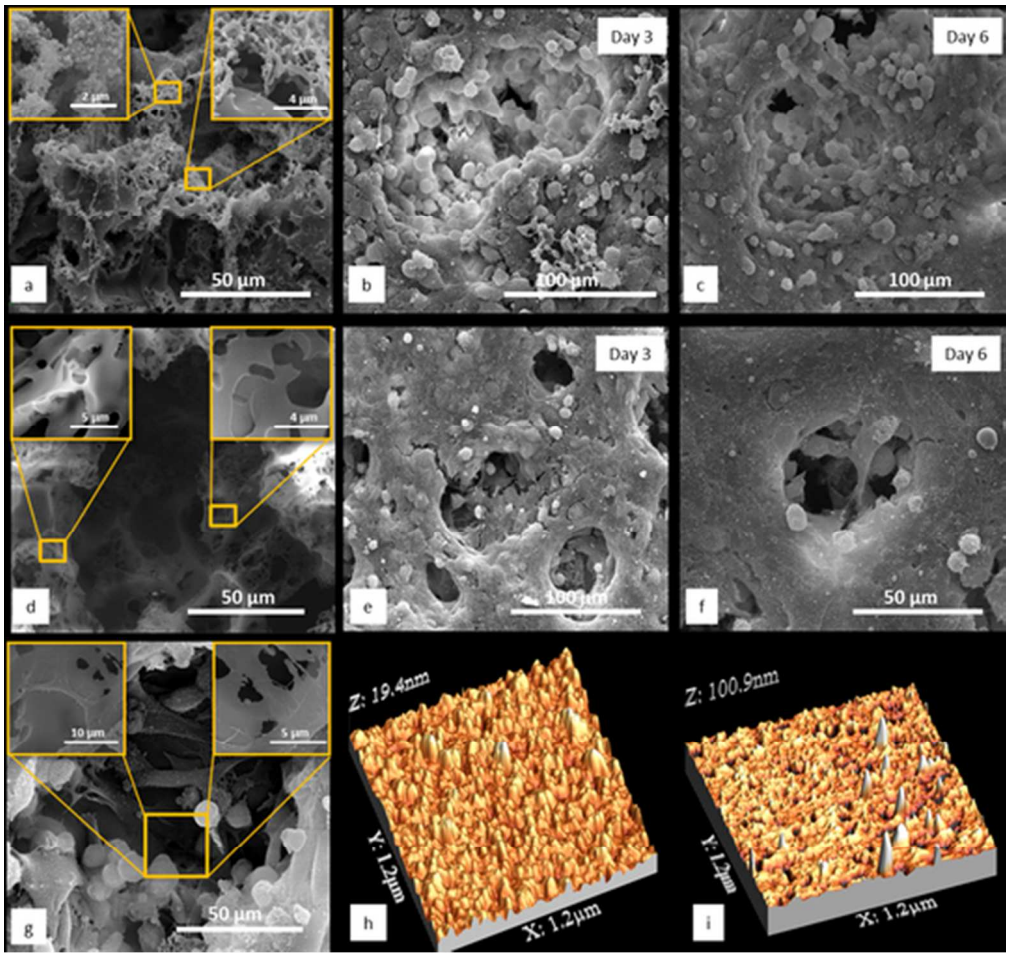

Figure 4. SEM micrographs of PLLA (a-c) and PS (d-f) scaffolds reveal different mechanisms employed by cell populations to fill pores. Scaffold A with pore size (104µm ± 4µm) was used. HepG2 tissues grown on PS scaffolds fill pores with an "outside-in" manner, while tissues on PLLA form a loose network termed "inside-out". Investigation of high magnification SEM micrographs of blank PLLA (a) and PS (d) scaffolds reveal differences in nanotexture inherent to the manufacturing process. Button- and Rod-like textures on PLLA appear randomly throughout the scaffold, while PS maintains a smooth surface with occasional 1 – 5 µm pores. Lamellipodia and filopodia were observed penetrating microporous structures in PS scaffolds (g). Part h and i show the 3D topographical images of a 1.2 x 1.2 µm2 area scan of NaOH-treated PS and PLLA scaffolds, respectively, obtained using AFM. A difference in surface roughness between the two surfaces can be observed at the nanolevel.

45x43mm (300 x 300 DPI)

This article is protected by copyright. All rights reserved.

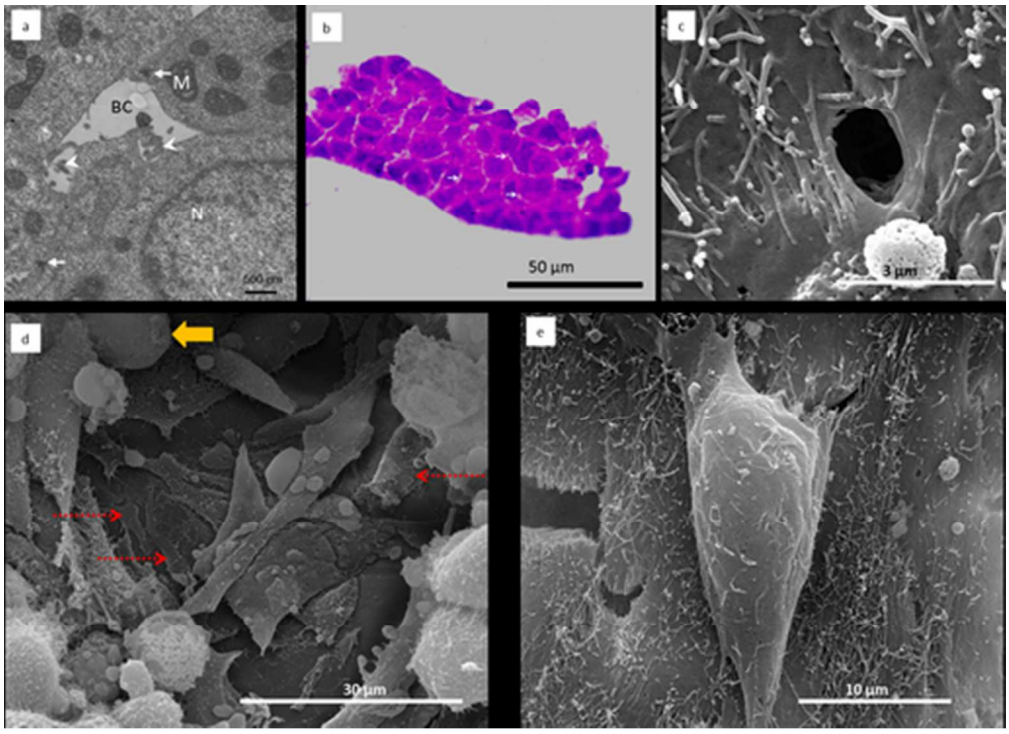

Figure 5. Structural characterization of HepG2 tissues using TEM (a), H&E (b), and SEM (c). These bile canaliculi-like structures are absent in 2D cultures, and serve as markers for CPR. Microvilli-lined canaliculi were observed using TEM on day 6 of culture (a). Multiple cell-cell junctions and canicular networks were observed in scaffolds. White solid arrow – tight junction, white arrowhead – microvilli, M – mitochondria, N - nucleus. H&E staining on day 6 showed high viability and development of channels (b; white arrows). Frequent opening of the channels on the surface of the microtissue (c). (d & e) show SEM images of HepG2 cell-material and cell-cell interactions on a porous PS scaffold. Consistent with current literature, cells adapt to the stiffness of their environment and adopt a flat, spread out morphology (d). However, cells that interact exclusively with other cells adopt a round morphology, suggesting the cell perceives a softer, in vivo-like stiffness (e).

43x31mm (300 x 300 DPI)

Acce

This article is protected by copyright. All rights reserved.